Analysis of crosstalk drift and optimization of spatial light modulator based mode-selective multiplexers for multimode fibers

ZUN HTAY,* D FABIO A. BARBOSA, AND FILIPE M. FERREIRA D

Optical Networks Group, Department of Electronic & Electrical Engineering, University College London, London WC1E 7JE, UK

*z.htay@ucl.ac.uk

Abstract: Adaptive mode-selective multiplexers offer the potential to control the modal content within multimode fibers for space division multiplexing (SDM). To such an end, spatial light modulators allow programmable control over the phase, amplitude, and polarization of optical wavefronts. One of the major challenges is to precisely match the manipulated beam to the waveguide modes in the multimode fiber. Achieving precise alignment of optical components within the free space system is crucial for accurate mode multiplexing while active alignment may be necessary to overcome environment induced drift. In this paper, we investigate, through theory, simulations and experiments, the impact of misalignment errors in a free space telescopic Fourier system, including phase mask and lenses misposition and angular misalignment in fiber collimation. Mode multiplexing is achieved using phase holograms in the Fourier domain while mode demultiplexing is achieved through off-axis holography and Fourier domain processing. Furthermore, we analyze the crosstalk drift with time in SDM transmission over a 45 mode OM3 fiber. System stability is experimentally evaluated over a 9-hour transmission period.

Published by Optica Publishing Group under the terms of the Creative Commons Attribution 4.0 License. Further distribution of this work must maintain attribution to the author(s) and the published article's title, journal citation, and DOI.

Introduction

The ever-increasing traffic demand in optical communication systems is exhausting the available bandwidth in single-mode optical fibers. To increase bandwidth density, space-division multiplexing (SDM) using multimode fibers (MMFs), few-mode fibers (FMFs), and/or multicore fibers (MCFs) has gained attention for the next multiplicative capacity growth in optical communications [1]. Among these, SDM in MMFs allows for the largest spatial density of information with a potential for several 100s of spatial modes in a conventional 125 µm fiber cladding [2]. However, computationally costly digital signal equalization techniques are required to overcome linear mode coupling in MMFs [3]. Motivated by the potential of programmable optics in hybrid equalization schemes that combine digital electronic and analogue optical signal processing [4,5], we consider the use of spatial light modulators (SLMs). SLMs can dynamically control optical wavefronts and selectively modulate specific combinations of spatial modes, providing enhanced mode launching and processing capabilities [6,7]. Recent advancements in high-refresh rate SLMs and machine learning-assisted techniques have significantly enhanced the efficiency and control of MMFs, providing promising directions for mode-multiplexing technologies [8,9]. While [10] and [11] explored methods for controlling the light propagation through MMFs by leveraging mechanical perturbations and optimal input excitations, showing promise for more robust mode-multiplexing systems Yet, aligning wavefront shaped beams with MMFs is a challenging task, requiring tedious system setup for optimal performance. SLM-based spatial multiplexing in MMFs suffers from various misalignment errors such as angular misalignments, lateral offsets, and axial displacements, among others, each contributing

to the degradation of the system performance by increasing modal crosstalk (XT) and reducing transmission efficiency [12,13]. These issues have been discussed in several research works. In [14], overcoming the challenges of imaging through MMFs by measuring the transmission matrix and using wavefront shaping techniques to control light propagation are discussed. The paper demonstrates that light propagation in MMFs can be predicted with up to 95% phase agreement, even for lengths of 300 mm. The authors achieved over 93% power conservation in the main diagonal of the transformation matrices after optimization, indicating strong preservation of light modes. Additionally, the study shows that even significantly bent fibers retain predictable behavior, with a curvature scaling factor of 0.77 ± 0.02 , closely aligning with theoretical models. Similarly in [9], the study achieved over 80% power efficiency in shaping the output optical field using SLM. The paper also provides quantitative results on the effectiveness of this technique in applications such as microparticle manipulation, demonstrating its practical viability in biophotonics. In [15] the impact of transverse misalignments in connectors is quantified, showing that a misalignment exceeding 18% of the fiber core radius can lead to more than 0.2 dB of mode-dependent loss (MDL). The study validates the coupling matrix through experiments and numerical simulations, demonstrating statistically significant degradation in signal quality due to mode coupling. [13] focused on optimizing an multi-plane light conversion (MPLC)-based mode multiplexer, achieving low insertion loss below -3 dB and minimal XT as low as -43.6 dB, with strong tolerance for fabrication and alignment errors, allowing for misalignments up to 30 µm without significant performance degradation.

While the aforementioned studies focus on overcoming fiber induced distortions, optimizing fiber connector design, enhancing mode control within the fiber, and improving the performance of an MPLC-based mode multiplexer with a primarily emphasis on error tolerance and performance under controlled conditions, our work takes a different approach by analyzing the long-term stability of an SLM-based mode multiplexer, finding that XT drifted by a few dB over 9 hours due to environmental factors like thermal drift and vibrations. Additionally, we provide a comprehensive examination of misalignments in a free-space optical setup. This adds an extra layer of insight and a performance quantification which are essential for the successful deployment of SDM technologies—an aspect not thoroughly addressed in existing research. Achieving meticulous alignment and implementing correction mechanisms are crucial for minimizing these errors and optimizing the fidelity of the modulated beam, improving system performance. The better the selectivity at launch/detection, the better one can implement optical processing for channel diagonalization techniques such as principal modes [16]. Moreover, in the SLM setup, a particular eigenmode of the overall fiber channel can be selectively excited by tailoring the SLM phase pattern, and ultimately the desired tributary mode exits the MMF for detection. However, in a fiber link subject to disturbances, the channel state changes over time and the phase pattern required to maintain mode orthogonality becomes invalid as the channel eigenmodes drift. This drift phenomenon is undesirable. The practical implementation of SLM spatial multiplexing faces challenges related to environment-induced drift effects, which can significantly degrade system performance over time. These variations can lead to fluctuations in the coupling efficiency and modal properties of the mode (de-)multiplexer and MMF, ultimately causing signal degradation and limiting the achievable transmission performance.

In this paper, we analyze different scenarios of conceivable misalignment in a mode-selective multiplexer built using a telescopic Fourier system and a phase-only SLM. The objective of this paper is to identify the most critical parameters and their tolerances for the free space system such that optimal performance can be obtained. Performance will be measured in terms of selective generation of linearly polarized (LP) modes – namely, those corresponding to an OM3 fiber profile. XT to non-targeted modes will be used as the key performance indicator. Moreover, this paper integrates and extends our previous work on XT drift in a SDM set up for a 45-mode MMF. Here, the mode (de-)multiplexer consists of an SLM in a Fourier Telescope arranged with

2898

the resulting diffraction field is transformed onto the facet of the MMF. We thoroughly analyze the drift in both the SLM-based mode multiplexer and the MMF over a prolonged period. We highlight the importance of precise alignment and the impact of misalignments, such as angular and axial offsets, on XT and overall system fidelity.

2. **Experimental setup**

Figure 1 describes the schematic diagram of the experimental free space optical setup where three lenses are used to Fourier transform the diffraction field produced by the SLM and projected onto the MMF fiber facet. The SLM used in this study is the Holoeye Pluto 2.1, a phase-only reflective liquid crystal on silicone (LCOS) SLM with a pixel pitch of 8 µm and an active area of 15.36 mm × 8.64 mm, comprising 1920 × 1080 pixels, with a fill factor of 93%. For the phase mask generation, a circular active area of approximately 800 pixels in diameter was utilized, supporting the accurate shaping of input beams to match the mode profiles required for OM3 fiber coupling. The SLM provides a full $0-2\pi$ phase modulation range at 1550 nm, and 90% reflectivity, enabling efficient mode multiplexing with minimal loss and XT. The experimental setup consists of three lenses which we terminologically described as objective, relay lens and microscopic objective (MO). The first two lenses (objective and relay lenses), with a focal length (f_{eff}) of 15 cm, are used as a relay telescope with no magnification to allow for a workable distance between the SLM and the MO. Otherwise, the MO would have to seat millimeters away from the SLM which would not be practical and potentially block the incoming beam from hitting the SLM. The MO is responsible for Fourier transforming the SLM diffraction field onto the fiber core and thereby, obtaining the desired amplitude and phase spatial distribution.

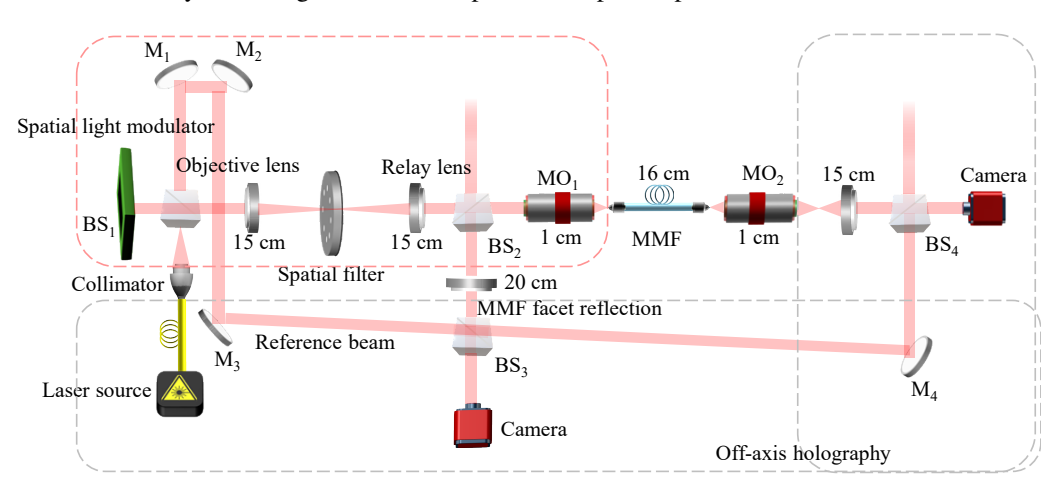


Fig. 1. Diagram of the experimental setup of the Fourier telescope free space optical system for spatial multiplexing.

Illumination of the SLM in Fig. 1 is achieved using a SMF with a numerical aperture (NA) of 0.14 and a beam collimator with a focal length of 37.5 mm - generating a beam of approx. 7 mm. The focal length of the MO (1 cm) is chosen to best utilize the SLM active area, and maximize the phase mask diameter on SLM, and match the targeted MMF core size 50 µm, the phase masks with 800 pixel diameter reach well into the MMF cladding allowing to resolve the evanescent field into cladding and preventing unwanted excitation of radiation modes. Holograms uploaded to the SLM are optimized using a direct search algorithm similar to [17]. The 45 LP modes of an ideal OM3 fiber at 1550 nm are the targeted replay field in our setup. The OM3 fiber under test, with a length of 16 cm, is connected at one end to MO₁ and to MO₂ at the other end. A standard OM3 fiber is used, this corresponds to a core radius of 25 µm, a cladding radius is 62.5 µm, a

relative core-cladding refractive index difference of 1%, and a core grading exponent around 2.1 - optimized for VCSEL-based transmission at 850 nm. This was a bend-insensitive fiber, thus includes a cladding trench – the associated minimum bend radius is around 7.5 mm. An InGaAs camera and an extra lens with a f_{eff} of 15 cm are used to view and capture the transmitted LPmodes. The camera has a resolution of 640×512 and a pixel size of 15 µm. We employ the off-axis holography method for the reconstruction and extraction of the amplitude and phase characteristics of the camera captures. The schematic depicted in Fig. 1 illustrates this approach, wherein the reference beam is generated via a beam splitter (BS₁) and a set of mirrors (M_1, M_2 , and M_3). Subsequently, it is combined with the object beam at a non-zero angle using BS_3 and BS₄ and M₄. Additionally, a spatial filter with a pinhole size of 800 µm is implemented to eliminate any artifacts present in the diffraction field generated at the SLM plane. For a rigorous analysis of the XT drift in the MMF, the XT drift of the optical system itself was measured by monitoring the reflection from the MMF facet. For this purpose, we used a camera with the same characteristics as before together with a lens of $f_{eff} = 20$ cm, composing a $20 \times$ telescope together with the MO₁ utilized. In our setup, we measured both the transmitted light and the reflected light, in turn. Specifically, when measuring the output of the MMF, we ensured that the reflected component was not interfering with the measurement. This was achieved by blocking the reflected path using a free-space attenuator. This approach allowed us to obtain precise measurements of the transmitted signal without the influence of reflected light.

Crosstalk analysis in spatial misaligned 4-F system

To better understand and analyze the experimental results obtained with the setup in Fig. 1, we first provide a theoretical and numerical analysis of several potential errors in the positioning of lenses. The analysis can be divided into that of the three 2F sub-systems that compose it. It is worth noting that these six scenarios can be logically grouped into two main cases: scenarios involving collimated light and those involving non-collimated light. For one 2F system, there are two distinctive axial distance offset errors: (i) $z_1 = f_{efl}$ and $z_2 \neq f_{efl}$, (ii) $z_1 \neq f_{efl}$ and $z_2 = f_{efl}$ - where z_1 and z_2 refer to the distance before and after the lens, respectively. These two cases have different impacts on phase sensitive imaging systems as ours. This can be understood using an operator approach based on [7] starting with the general case, where z_1 and z_2 are arbitrary. Following the operator method, free space propagation of a field U(x) over a distance z is given as $R[z] = \frac{1}{\sqrt{iAz}} \int_{-\infty}^{\infty} U(x) \exp(ik(x-u)^2/2z) dx$.

When a lens is applied to a field U(x), a quadratic phase exponential Q of the form Q[c] = $exp(ikcx^2/2)$ U(x) is introduced, where $c = 1/f_{eff}$. In this way, propagation over z_1 , a lens, and over z_2 , can be expressed as $R[z_2]Q[c]R[z_1]$. We can now simplify this composed operator for the two scenarios above. Before doing so, just to note that for a perfect 2F configuration, $z_1 = z_2 = f_{eff}$, the general expression can be reduced to $\mathcal{V}[1/\lambda f] \cdot F$, basically corresponding to a scaled Fourier transform, where \mathcal{V} is the scaling operator given by $\mathcal{V}(b) = \sqrt{|b|} U(bx)$ and is the Fourier transform given by $F = \int_{-\infty}^{\infty} U(x) \exp(-2\pi ux) dx$. For case (i), $z_1 = f_{efl}$ and $z_2 \neq f_{efl}$, i.e., a misaligned replay field, the general case operator simplifies to $\mathcal{V}[1/\lambda f] \cdot R[(z_2 - f)/\lambda^2 f^2] \cdot F$, making it clear that we no longer have a scaled Fourier transform due to the diffraction term introduced by the R operator. Importantly, if a defocus Zernike Q term is added to the SLM diffraction field it can be shown that the R term can be cancelled. For case (ii), $z_1 \neq f_{efl}$ and $z_2 = f_{efl}$, i.e. misaligned diffraction field, the general case can be simplified to $V[1/\lambda f] \cdot Q[\lambda^2(f-z_1)] \cdot F$, corresponding to a Fourier transform followed by a quadratic phase exponential term. Unfortunately, this O term cannot be cancelled via a correction to the SLM diffraction field. Therefore, if the phase of the Fourier transform is crucial, as it is here, precise positioning of the SLM one focal length away from the lens becomes indispensable, as Zernike corrections at the diffraction field plane are insufficient for addressing this specific misalignment. Nevertheless, if only the amplitude of the replay field is of importance the Q term is not relevant. In the following we will analyze the

impact of these positioning errors on the XT between modes in the context of SDM. Six scenarios concerning axial positioning offsets in lenses are analyzed here to address critical points in the telescopic system where misalignments can have significant implications for overall performance – given the insight developed earlier on using the operator approach. For these scenarios, we estimated the XT performance for all cases by sweeping the error in z_1 and z_2 (*Note*: We also verified that these changes did not influence the analysis through the spatial filter by evaluating the system with and without corrections applied to the spatial filter, while simultaneously adjusting the lens positioning).

Figure 2(a)-(f) show the optical system configuration for scenarios 1 to 6, respectively. Scenario 1 examines the misalignment at the entrance (objective lens), while scenario 2 investigates misalignments at the exit of the system, this is at z_1 and z_2 for the MO lens, where the fidelity of the replay field is directly impacted. Scenarios 3 and 4, consider the compounded error of two consecutive lenses. And finally, scenarios 5 and 6, consider errors in all three lenses, addressing global alignment issues crucial for accurate imaging throughout the system. In these cases, and from the operator method, we expect a misalignment in z_2 to have a larger impact than those in z_1 , given their direct impact on the replay field fidelity towards a given target field.

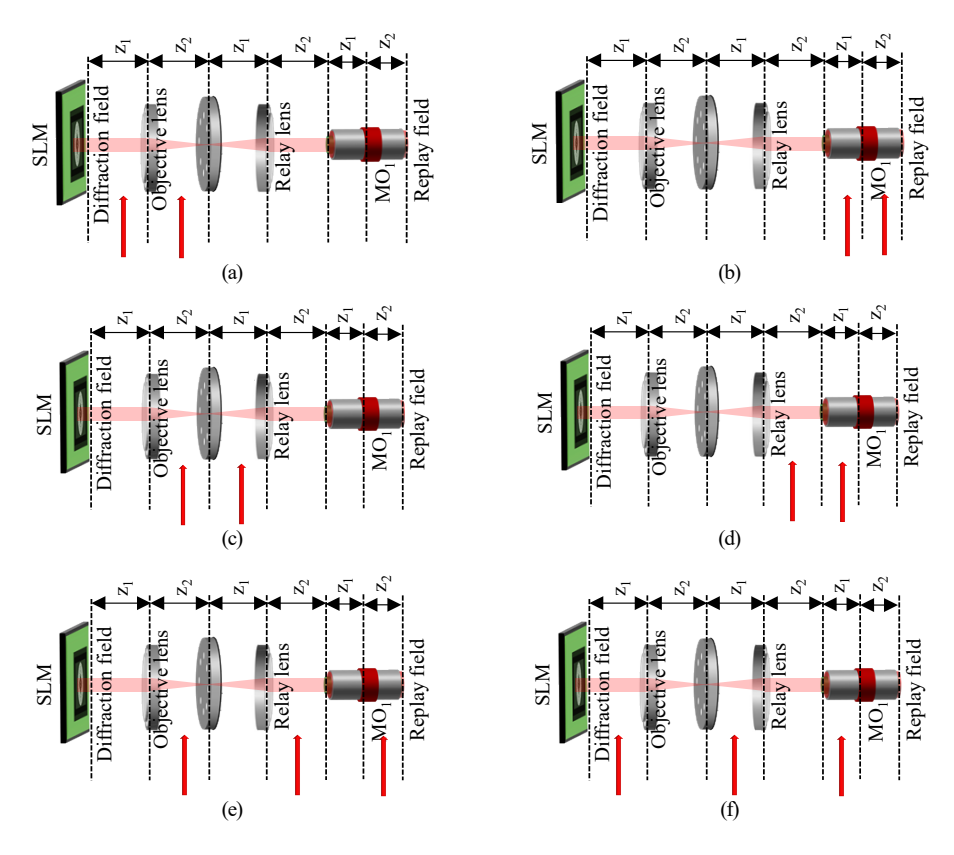


Fig. 2. Spatial misalignment in (a) ConFig. 1: z_1 and z_2 of objective lens, (b) ConFig. 2: z_1 and z_2 of MO lens, (c) ConFig. 3: z_2 of objective lens and z_1 of relay lens, (d) ConFig. 4: z_2 of relay lens and z_1 of MO lens, (e) ConFig. 5: z_2 of all three lenses, (f) ConFig. 6: z_1 of all three lenses.

The XT in the following is calculated as the power in the desired mode relative to the total power in all other modes. And, to neglect the intra-mode group mixing effect, XT is averaged among all outputs of the same mode groups as in [18]. Note that, intra-mode group mixing can

be addressed through electronic compensation [16]. The mode-to-mode XT, from an input mode $LP_{n,m}$ to the output given by $LP_{k,l}$ is written as:

$$XT_{LP_{n,m}\to LP_{k,l}}^{MG} = \frac{\sum_{u+2v=k+2l} P_{(n,m)\to(u,v)}}{(k+2l-1)\sum_{p+2q=n+2m} P_{(n,m)\to(p,q)}}.$$
 (1)

Furthermore, the *mode-group-to-mode-group XT* between an input mode group (MG_i) and an output mode group (MG_k) , can be calculated as:

$$XT_{MG_{i} \to MG_{k}} = \frac{\sum_{u+2v=k \land n+2m=i} P_{(n,m) \to (u,v)}}{k \cdot i \sum_{p+2q=i \land n+2m=i} P_{(n,m) \to (p,q)}}.$$
 (2)

Figures 3(a)-(f) present the resulting averaged XT per mode (starting with (1)) corresponding to spatial errors in the scenarios described in Fig. 2(a)-(f), respectively. Note that even with perfect positioning of all lenses, Fig. 3 indicates that the best mode averaged XT achieved is around -35 dB given that the holograms have finite resolution. Figure 3(a) shows, for the objective lens, that a spatial error of >3 mm in z_2 can degrade the XT by approximately ~5 dB while there is almost no impact from z_1 even for offsets as large as 5 mm. Figure 3(b) shows XT against z_1 and z_2 errors for the MO, where z_2 misalignments cause noticeable degradation, while z_1 errors < 60 μ m have minimal effect. This is due to the shorter length of the MO (10 mm rather than 150 mm for the other lenses) where; the impact of misalignment quickly grows beyond 10 μ m from -35 dB up to -20 dB (at 60 μ m).

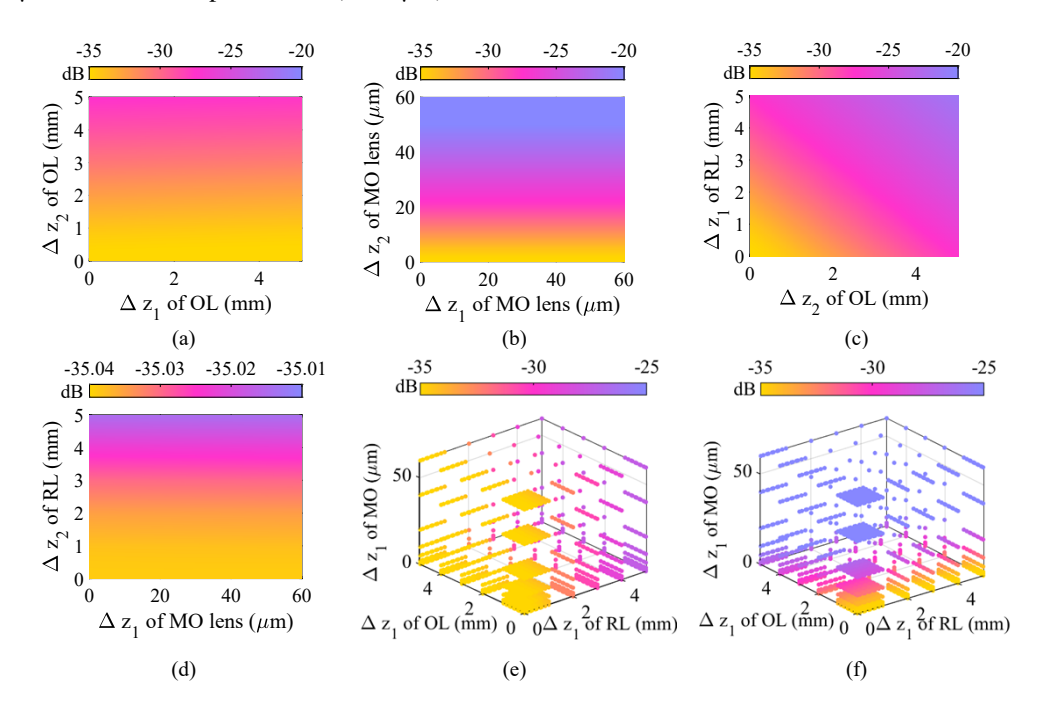


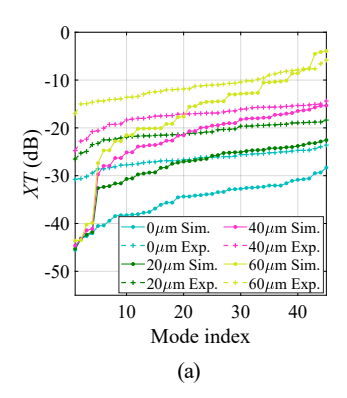
Fig. 3. Spatial misalignment versus average *XT* as a function of *LP* modes in (a) ConFig. 1, (b) ConFig. 2, (c) ConFig. 3, (d) ConFig. 4, (e) ConFig. 5, (f) ConFig. 6. These configurations correspond to those presented in Fig. 4(a)-(f). OL, RL and MO refer to objective lens, relay lens and microscopic objective, respectively

Figure 3(c) presents the average XT in case there is a compounded positioning error in the first two lenses. It is observed that for a positioning error beyond 2 mm there is a steep increase on

XT with errors in any of the two lenses. Figure 3(d) shows XT given an error in the separation between the relay lens and the MO. There is only a negligible change in XT in the error between the z_2 of relay lens and z_1 of MO lens. The performance of this scenario (4) is unexpected given that a large z₂ error leads to minimal XT degradation. This can be explained by the combination of general operators for misaligned $z_2 \neq f_{eff}$ in relay lens and $z_1 = f_{eff}$ in MO lens, simplified to $\mathcal{V}[-1/\lambda f_{MO}] \cdot Q \left[-\lambda^2(\varphi - \varphi_{MO})\right] \cdot F$, where $\varphi = z_{2(relay)} - f_{relay}$ and $\varphi_{MO} = z_{1(MO)} - f_{MO}$. The simplified equation is comparable with a single lens misaligned diffraction field case where the z_1 misalignement has less (i.e., only phase) effect on the replay field. Hence, a reduced impact in XT.

In Fig. 3(e) and (f), we analyzed the spatial errors in z_1 and z_2 of all three lenses, respectively. Figure 3(e) shows that z₁ of relay lens has the most critical alignment requirement, with negligible impact from other lenses (z_1) . Figure 3(f) indicates that since z_2 has the more prominent effect on misalignment in all lenses, except in relay lens. In three lens telescopes, z₂ of the shortest focal length lens (MO) is expected to be the most sensitive to misalignment compared to the other two lenses. Due to this reason, we focused our further analysis on the most critical part of the overall system and included the experimental analysis.

Figure 4 shows (a) the XT per mode using (1) and (b) the maximum mode-group-to-mode-group XT using (2), for experimental and simulation with spatial errors in the z_2 of the MO. Figure 4(a) shows that the XT performance, for a given system configuration, can differ as much as 10 dB between the worst and best mode. There is a significant difference in performance between simulation and experiment, about 5 dB, although the XT vs mode trends are in qualitative agreement. This differential is likely due to residual alignment issues, angular misalignment, lens aberrations, and/or SLM artifacts. This observation aligns with the closer agreement between simulation and experiment when a large z₂ error is intentionally introduced (reducing the relevance of rather unavoidable experimental residual misalignments). Figure 4(b) shows the comparison of experimental and simulation results for maximum MG to MG XT with 0, 20, 40 and 60 µm spatial error. Here it is even more clear that the resulting XT performance in the experiment follows a similar trend to the simulation with larger degradation. The XT in the experiment for baseline (0 µm) in which, the system is precisely aligned as much as possible has similar XT performance compared to the 20 µm of spatial error in the simulation.



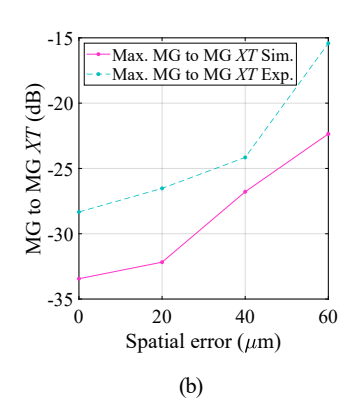


Fig. 4. Spatial error versus (a) XT as a function of LP mode index (modes ordered by increasing XT). (b) Maximum MG to MG XT for experimental and simulation.

In comparing the experimental results with the simulation in Fig. 4, we note an absolute difference. This can be explained by the misalignments modeled in Fig. 3. While it is not possible to precisely determine the actual z₁ or z₂ misalignments for each lens, we verified that a

reasonable match between experiment and simulation is achievable by arbitrarily adjusting these values. This suggests that alignment discrepancies are likely the primary source of error.

4. Crosstalk analysis in phase mask and angular misaligned 4-F system

Besides potential offsets on lenses axial positioning, there are other sources of wavefront shaping errors. In an ideal scenario, the Gaussian beam collimated from the launch SMF is accurately centered and aligned when projected over the hologram. In reality, the input beam may hit the SLM off-center with regards to the hologram. We model such misalignment by offsetting the hologram position in the SLM in both the X and Y directions, see Fig. 5(a). This is expected to lead to loss of holographic features which can result in lower fidelity of the replay field and excess XT between spatial modes. Figure 5(b) illustrates the averaged XT of 45 modes with pixel shifts. Each pixel is assumed to have a size of 8 μ m, with the X and Y axes denoting the directional shift in pixels. It is observed that the alignment in this context is remarkably delicate, alignment must be precise and should be smaller than 1 pixel – mode selectivity is fully lost for shifts larger than 2-4 pixels.

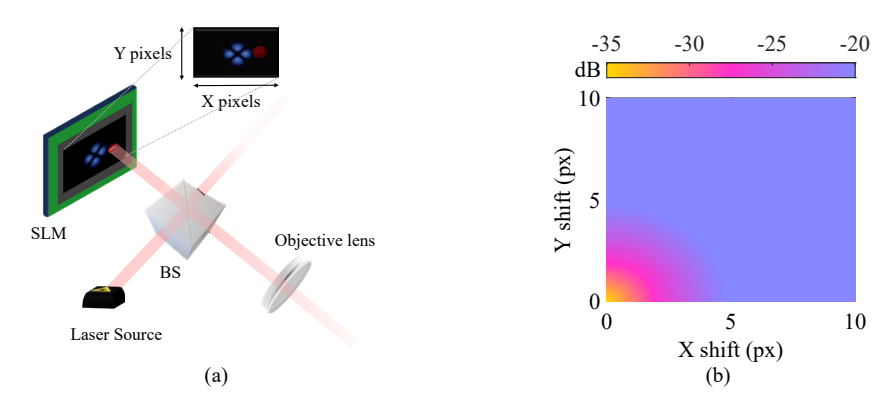


Fig. 5. (a) Beam positioning misalignment to the SLM as a function of SLM pixels and (b) average *XT* over pixel shift in the X and Y direction.

Another potential misalignment is that between the focused beam from the MO and the MMF core plane, where the output beam of the MO is not normal to interface the MMF facet, see Fig. 6(a). This misalignment can be approximated by a linear phase ramp to the beam wavefront and can be described as:

$$H'(x, y) = H(x, y) \exp(-ix.\sin(\theta) \cdot 2\pi/\lambda)$$
(3)

where H' is the distorted replay field, H is the target mode field distribution, x and y are the spatial cartesian coordinate, θ is the angular tilt (from the normal to the MMF facet) in radians and $2\pi/\lambda$ is the wavenumber – assuming a phase ramp along x. Angular misalignment and the consequent linear phase ramp distortion will affect the mode selectivity. Figure 6(b) shows the angular misalignment in x direction (x tilt) and in y direction (y tilt) versus average x. It is noted that a small degree >1 ° can degrade the system significantly with the slope of x of 5 dB/0.5°. This can be mainly due to the misalignment introducing distortions in phase while the intensity of the desired mode is maintained.

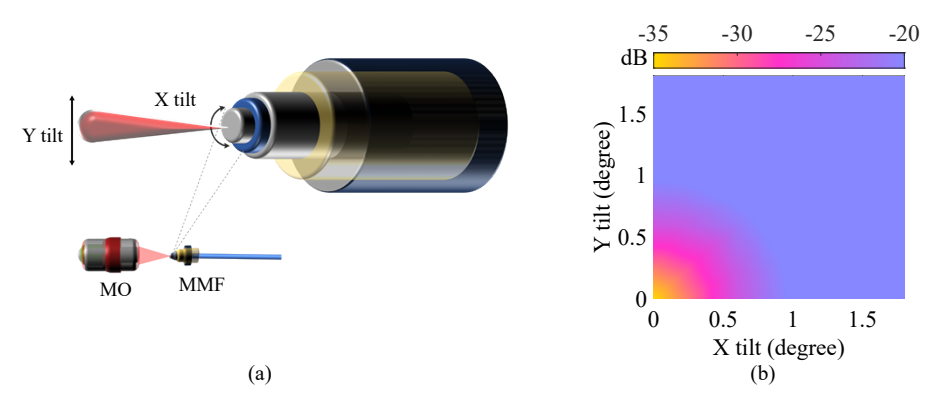


Fig. 6. (a) Propagated beam with angular misalignment before being coupled into the MMF core and (b) average *XT* over angular misalignment in degree.

5. Crosstalk drift over time in SLM-based systems

Here, we experimentally investigate the XT drift of our SLM-based spatial multiplexing system, see Fig. 1. To better understand the experimental results, the analysis comprises the characterisation of the drift of free space Fourier telescope and of that of the MMF. In our previous work, we numerically investigated the static spatial misalignment that has a cumulative impact on overall system performance [19]. Here, we evaluate the stability of the system by monitoring the system modal XT change over time. The modal XT can be calculated as the ratio between the average power of undesired modes and the remaining power within a specific set of modes – assuming the launch is intended solely on the chosen set of modes.

A standard circular core MMF is used in this experiment, therefore the coupling first occurs within mode groups, and then across neighboring groups. For that reason, the use of mode group division multiplexing has been proposed before. In this context, the inter-mode group XT, and its variation with environment conditions, are of particular interest. For a certain mode group, and over a certain fiber/device, the XT in the following is calculated as before.

Figure. 7(a)-(d) show the measured 45 LP mode transmission matrix of the LP modes in the mode multiplexer and the MMF transmission where the x and y axis run from mode 1 ($LP_{0,1}$) to mode 45 ($LP_{0,5}$). We observed the system performance by constantly capturing data for 9 hours. These two scenarios are being assessed and recorded separately over equal durations but in different timelines (only one InGaAs camera was available). Figure 7(a) and (b) correspond to the SLM-based mode multiplexer (only) after 1 and 9 hours, respectively. It can be seen that, that the coupling matrix for the mode multiplexer is of good selectivity (\sim 20 dB) – limited by SLM resolution and residual alignment errors. An error as small as 5 μ m in the MO positioning can lead to a \sim 1 dB χ 7 penalty [19]. The residual interference terms correspond to mode pairs with large modal overlap. After 9 hours, the coupling matrix in Fig. 7(b) shows a measurable χ 7 increase (few dB).

Furthermore, Fig. 7(c) and (d) depict the transmission measurement including the fiber under test at the 1st and 9th hour. The process of launching a specific mode in a fiber leads to larger XT, even for just 16 cm, mainly among modes of the same mode group. This is due to the fiber coupling. Note that small fiber imperfections lead to strong mixture of degenerate modes, e.g., LP_{11a} and LP_{11b} . Also, the XT is larger for higher-order modes given their more intricate spatial distribution (thus, higher spatial frequencies). Figure. 8 depicts the inter-mode group XT vs time over the whole 9 hours (averaged over all mode group combinations): for the mode multiplexer (only) and for MMF transmission. It can be seen that the XT is fairly stable, in both cases particularly in the absence of fiber, until a couple of XT surges (\sim 1 dB) beyond 5 hours.

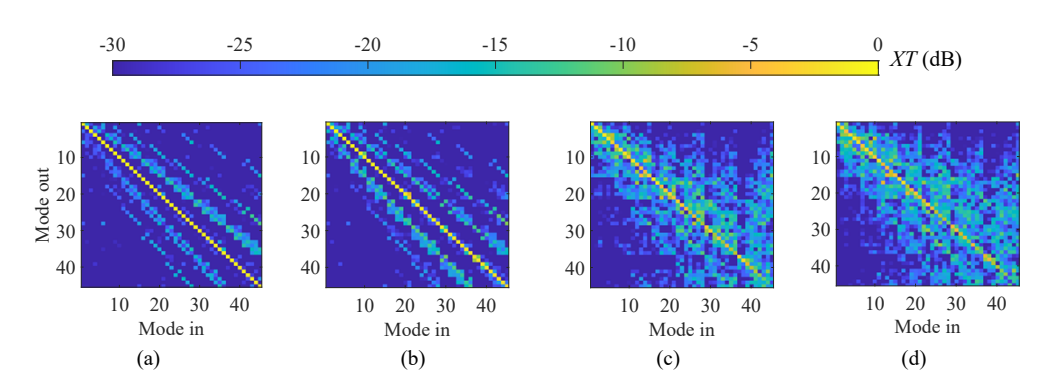


Fig. 7. The measured coupling matrix between 45 *LP* modes transmission of SLM-based mode multiplexer in (a) 1 hour, (b) 9 hours, and of MMF transmission in (c) 1 hour, (d) 9 hours.

This can be explained by a combination of thermal drift (4°C monotonic increase over the whole period) and vibration induced by a busy laboratory environment. It is known that, for the optical mounts used, temperature variations can cause irreversible shifts in position from the fluid flow of grease and the unrelieved stress in kinematic seats and flexure stages – directly affecting the free space setup. Using a miniaturised setup with fixed structures, similar to commercial devices should reduce the environmental-induced drift. The XT surges in both lines in Fig. 8(a) do not align since these are different captures as only one InGaAs camera was available. However these results were captured in similar conditions over consecutive days, during the same time period, without room climate control. The similar trends in both lines seem to indicate that the average inter-mode group characteristics of the fiber are relatively stable, and the XT jumps beyond 5 hours are related with the mode (de-)multiplexer drift. Moreover, the average XT within the mode groups in MMF transmission performed similarly to OM2 fiber utilized in [20].

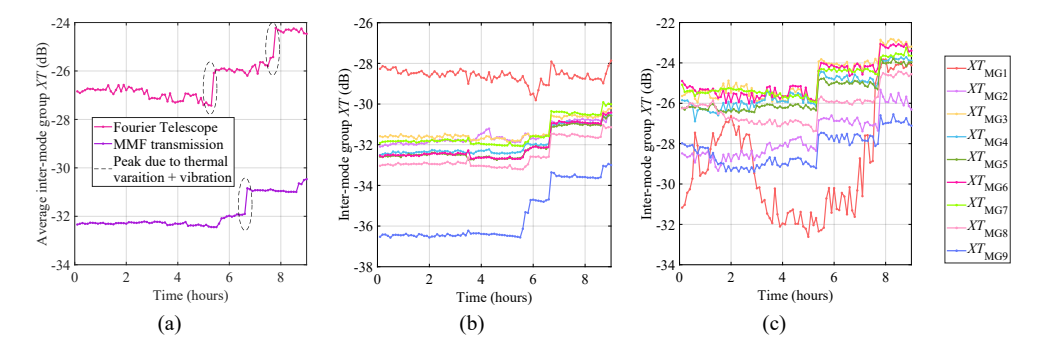


Fig. 8. (a) The Inter-mode group average XT over time in the SLM-based mode multiplexer and MMF transmission. The inter-mode group XT over time (b) in mode multiplexer, and in (c) MMF transmission.

Figure. 8(b) and (c) display the inter-mode group XT over time for the mode multiplexer and for the MMF, respectively. In this case, XT_m is presented, with $m = \{MG1, ..., MG9\}$. Over the first 5 hours, in the mode multiplexer only, XT_{MG9} and XT_{MG1} exhibits the most variation in mode multiplexer and MMF transmission respectively, where all the other mode groups remain stable within a ~ 1 dB peak-to-peak variation. In Fig. 8(c), it can be seen that XT_{MG1} experienced significant variation, ~ 6 dB, in the first 5 hours, while the other modes remained relatively stable. The variation in XT_{MG1} can be understood by noting that LP_0 m modes share a large spatial mode

overlap, therefore coupling to and from $LP_{0,1}$ is likely to be affected with any drift/deviation in the launching conditions into the fiber. The XT_{MG2} performed exceedingly well compared to other mode groups within -28 dB while XT_{MG3} remained stable at -25 dB. Before the 1st XT jump at 5th hour, which resulted in ~2.5 dB XT degradation in all mode groups, $XT_{MG4,6,7}$ and XT_{MG8} trends fluctuated within -25 and -27 dB whereas, XT_{MG2} and XT_{MG9} appear to perform with almost the same trend at 1 dB difference. After the 2nd XT jump, all mode groups continued to remain constant with an overall XT deviation of ~1 dB. We observe that the system stability could be further enhanced without the peaks attributed to the high activity within the laboratory environment.

6. Conclusion

We investigated the misalignments in a three-lens Fourier telescopic system, along with the XT drift over 9 hours, for an SLM based mode-multiplexer on its own and also when including MMF transmission. This study addressed the XT associated with misfocus from lens displacement, phase errors from inaccurate beam interaction with the SLM phase mask, and angular misalignment through theoretical, simulation, and experimental approaches. The mode multiplexer tolerance to various impairments and their combinations was tested. We investigated that some of the major sources of performance degradation are the alignment between the input collimated beam center and the SLM hologram center, the angular alignment between the projected replay field and the optical fiber facet, as well as the distance between the MO and the optical fiber facet. Interestingly, it was also found that the alignment of relay lens in the Fourier telescope is not as critical as that for the objective or MO lenses – this is positioning errors of as much as 3% are tolerable. The findings on system resilience to errors provide valuable insights for optimizing performance and minimizing XT in practical optical communication applications. Furthermore, the pre-liminary analysis of the XT drift over time has shown that, in the multiplexer and in the MMF, the XT drift appears to be stable in the overall – but for longer term stability (beyond a few hours) a fixed optical system is necessary. Further characterisation work for longer fiber lengths is planned.

Funding. UK Research and Innovation (MR/T041218/1).

Disclosures. The authors declare no conflicts of interest.

Data availability. Data underlying the results presented in this paper are not publicly available at this time but may be obtained from the authors upon reasonable request.

References

- D. J. Richardson, J. M. Fini, and L. E. Nelson, "Space-division multiplexing in optical fibres," Nat. Photonics 7(5), 354–362 (2013).
- 2. F. M. Ferreira and F. A. Barbosa, "Maximizing the capacity of graded-index multimode fibers in the linear regime," J. Lightwave Technol. **42**(5), 1626–1633 (2024).
- 3. B. Inan, B. Spinnler, F. Ferreira, *et al.*, "DSP complexity of mode-division multiplexed receivers," Opt. Express **20**(10), 10859 (2012).
- F. M. Ferreira, F. A. Barbosa, A. Ruocco, et al., "Scaling up SDM transmission capacity," in Photonics Conference, 13-17 1–2 (IEEE, 2022).
- D. Pohle, F. A. Barbosa, F. M. Ferreira, et al., "Intelligent self calibration tool for adaptive few-mode fiber multiplexers using multiplane light conversion," J. Eur. Opt. Society-Rapid Publ. 19(1), 29 (2023).
- 6. N. Savage, "Digital spatial light modulators," Nat. Photonics 3(3), 170–172 (2009).
- 7. J. W. Goodman, Introduction to Fourier Optics. W. H. Freeman, (2005).
- 8. H. Cao, T. Čižmár, S. Turtaev, *et al.*, "Controlling light propagation in multimode fibers for imaging, spectroscopy, and beyond," Adv. Opt. Photonics **15**(2), 524–612 (2023).
- T. Čižmár and K. Dholakia, "Shaping the light transmission through a multimode optical fibre: complex transformation analysis and applications in biophotonics," Opt. Express 19(20), 18871–18884 (2011).
- R. Shekel, K. Sulimany, S. Resisi, et al., "Tutorial: How to build and control an all-fiber wavefront modulator using mechanical perturbations," JPhys Photonics 6(3), 033002 (2024).
- 11. K. Wisal, C.-W. Chen, P. Ahmadi, *et al.*, "Suppressing Nonlinear Instabilities in Multimode Fibers via Wavefront Shaping," in *CLEO* (Optica Publishing Group, 2024) paper SM2E.5.

- 12. N. Patel and C. Narayanamurthy, "Measurement of optical misalignment using wavefront sensing," Opt. Eng. **54**(10), 104106 (2015).
- 13. J. Fang, J. Bu, J. Li, *et al.*, "Performance optimization of multi-plane light conversion (MPLC) mode multiplexer by error tolerance analysis," Opt. Express **29**(23), 37852–37861 (2021).
- M. Plöschner, T. Tyc, and T. Čižmár, "Seeing through chaos in multimode fibres," Nat. Photonics 9(8), 529–535 (2015).
- J. Vuong, P. Ramantanis, Y. Frignac, et al., "Mode coupling at connectors in mode-division multiplexed transmission over few-mode fiber," Opt. Express 23(2), 1438–1455 (2015).
- 16. F. A. Barbosa and F. M. Ferreira, "On a Scalable Path for Multimode SDM Transmission," J. Lightwave Technol. **42**(1), 219–228 (2024).
- 17. R. Mouthaan, P. J. Christopher, J. Pinnell, *et al.*, "Efficient Excitation of High-Purity Modes in Arbitrary Waveguide Geometries," J. Lightwave Technol. **40**(4), 1150–1160 (2022).
- 18. S. Bade, B. Denolle, G. Trunet, *et al.*, "Fabrication and Characterization of a Mode-selective 45-Mode Spatial Multiplexer based on Multi-Plane Light Conversion," arXiv (2019).
- 19. Z. Htay, F. A. Barbosa, and F. M. Ferreira, "On the effect of spatial misalignment analysis on spatial light modulator-based spatial multiplexing in multimode fibres," *CLEO* (2024).
- 20. S. Bade, B. Denolle, G. Trunet, et al., "Fabrication and Characterization of a Mode-selective 45-Mode Spatial Multiplexer based on Multi-Plane Light Conversion," in *Optical Fiber Communication Conference Postdeadline Papers* (Optica Publishing Group, 2018), paper Th4B.3.